Accurate determination of interfacial thermal resistance inside particle-laden composites based on high-throughput computation and machine learning

Xiaoxin Lu[#a], Jiabin Huang[#a], Nan Cheng[b,c], Linlin Ren[a], Jianbin Xu[d], Jibao Lu[a,b,*], Rong Sun[a,b]

[a]*Shenzhen Institute of advanced electronic materials, Shenzhen Institutes of Advanced Technology, Chinese Academy of Sciences, Shenzhen 518103, P.R.China.*
[b]*Shenzhen Institutes of Advanced Technology, Chinese Academy of Sciences, Shenzhen 518103, P.R.China.*
[c]*School of Electronic Science & Engineering, Southeast University, Nanjing, P.R.China*
[d]*Department of Electronics Engineering, The Chinese University of Hong Kong, Shatin, New Territories, Hong Kong 999077, China*

Abstract

Particle-laden composites are typical thermal interfacial materials (TIMs) in the electronic applications, which are widely used in the electron packaging fields. The effective thermal conductivity (effective TC) of the particle-laden composites is dominant by the particle-matrix and particle-particle interfacial thermal resistance (ITR). The reliable identification of ITR is essential for the accurate prediction of TC of the composites, which has potential in the design of TIMs. In this work, we propose an efficient strategy to identify the interfacial thermal resistance in the particle-laden composites combining the numerical simulation, high-throughput computation, machine learning algorithm and simple experimental measurement. Firstly, the high-throughput computation is conducted based on the numerical modeling of the standard samples, in which the input parameters are ITRs in the composites. Afterwards, a prototypical function-based machine learning strategy is employed on the database to describe the numerical relation between the effective TC and the input parameters. Finally, comparing the numerical predictions from the machine learning model with the experimental measurement of the effective TC, a high-throughput screening of the ITRs is

---

[*]Corresponding author *Email: jibao.lu@siat.ac.cn*

executed for the identification of their values. The reliability of the strategy is validated by an example of Al_2O_3-AlN/silicone composites, showing that the particle-particle ITR is higher than particle-matrix ITR.

1. Introduction

The increasing density of integrated circuit leads to a dramatic increase of heat accumulation per unit area of chip, making heat dissipation a bottleneck problem for electronic packaging [1]. To improve the thermal management as well as to enhance the lifetime and reliability of the device, thermal interface material (TIM) is filled into the gap between the chip and heat spreader to enhance the heat transfer [2, 3]. As required by the packaging processes, the high-end TIM in direct contact with the chip, termed as TIM1, is mostly composed of polymer matrix filled with thermally conductive particulate fillers. The polymer matrix, usually silicone-based polymers, provides the mechanical properties and workability of the composite material, while the particulate fillers are added to increase the effective thermal conductivity (effective TC). The efficient heat transport of the composite material relies on the formation of heat transfer paths due to the fillers. In order to facilitate the heat transfer, the fillers are selected as the ones with high TC, such as Al_2O_3 and AlN. When heat passes through the interface between different components inside the composite material, the temperature suffers a discontinuous jump; the ratio of the temperature discontinuity to the heat flux density through the interface is defined as the interfacial thermal resistance (ITR) [4], which is also known as Kapitza resistance [5]. The ITR significantly hinders the heat transfer at the interfaces, which leads to dramatic decrease of effective TC of composite material. As a result, though a variety of fillers with high TCs are used in the polymer-based composites, the resulting effective TCs of those materials are often far below those of the fillers and the expected values [6]. As the ITR plays a dominant role in determining the TC of polymer-based composite materials, it should be a key parameter to be considered when using analytical/empirical equations or numerical simulations to accurately predict the TC of a composite material. The theoretical/numerical prediction, if meets the requirement of accuracy,

2

could be a powerful tool to assist the design and engineering of composite materials with high TCs and other properties related to the performance.

There are several kinds of approaches to identify the ITR, including the theoretical phonon models, computer computations, direct experimental measurements, mining from the existing experimental data, and method based on calibration between models and experimental observables. The phonon-based models include the acoustic mismatch model (AMM) and diffuse mismatch model (DMM) [5]. For instance, Prasher [7] incorporated the van der Waals bonding parameters into AMM to model the contact resistance between nanoparticles and substrate surface. Reddy [8] calculated the thermal conductance of Al-Si, Al-Ge, Cu-Si and Cu-Ge interfaces over a wide range of temperatures by DMM model taking into account the full phonon dispersion relationship over the entire Brillouin zone. However, AMM works well only at very low temperatures since it ignores the scattering of photons at interface, and DMM is not suitable for non-elastic circumstances because the interfaces are assumed to be smooth and inelastic scattering was not considered. The complex structures and physical/chemical environments of the interfaces inside the composite material also prohibit the use of a phonon-based model to accurately calculate the ITR.

The computer computations for predicting the ITR includes the First Principles Calculation and molecular dynamics (MD) simulation. The former calculates the ITR based on quantum mechanics, which is accurate but prohibitively expensive when dealing with complex interface structures. The latter employs classical mechanics for the interatomic interactions to dramatically reduce the computational cost, which enables simulations of much larger systems. Many researchers have used MD simulations to calculate the ITR [9–13], with particular attention paid to understanding the mechanism of interfacial heat transfer. For instance, Ren et al.[9] investigated the ITR between carbon nanotube and aluminum substrate by two-temperature model along with non-equilibrium MD, in which the electrons and phonons are assigned into electronic and atomic subsystems respectively in order to include the contributions of both electrons and phonons. Meng et al.[10] studied the ITR between packed silica nanoparticle by using MD simulations and identified the critical role of chemical bonds between the nanoparticles in affecting the ITR. Nevertheless, it should be noted that the quantitative accuracy of MD simulation is not guaranteed because the force field based on artificial/empirical elements inevitably introduces arbitrary uncertainties

The direct experimental measurement of ITR were carried out by taking

3

advantage of the techniques such as 3ω method [14], laser flash technique [15], time-domain thermos-reflectance (TDTR) [16], hot-wire technique [17], infrared imaging technique [18], laser-flash Raman mapping [19], and thermal bridge method [20]. 3ω method, laser flash technique, TDTR and hot-wire technique identify ITR by controlling the heating of the samples followed by analyzing the generated 'electrical-thermal' response, whereas infrared imaging technique only takes advantage of the thermal information for the identification of ITR. Those methods are generally cumbersome due to the requirement of specific experimental devices and corresponding mathematic models for various composites. The laser flash Raman mapping and thermal bridge methods have been employed to measure the ITR between fibers which requires the extraction of two overlapping thermally conductive fillers. Recently, Fitzgerald et al. [20] measured the contact thermal resistance between Ag nanowires (AgNWs) with a PVP interlayer by using thermal bridge method. They found that the ITR between AgNW and PVP is significantly lower than that between the carbon nanotube (CNT) and typical polymers, which implies the higher efficiency of using AgNWs than CNTs as fillers in building heat-transfer paths in composite materials. Those works highlight the advances in the direct measurement of ITR as well as in understanding the underlying mechanism of thermal transport. The bottleneck is that experiments suffer from sample preparation for in-situ measurement, which is almost impossible to faithfully represent the complex physical and chemical environment of the nanoscale interfaces inside the composite material.

With the development of machine learning technique, prediction of ITR in various material systems based on mining from the existing experimental data attracts a lot of attention. Wu et al. [21] predicted the ITR for over 80,000 material systems composed of 293 materials by machine learning based on 1317 experimental data of 456 interface samples. The LSBoost, support vector machines (SVM) and Gaussian Regression Processes (GPRs) algorithms were used for the models, with the material properties, compositions, and chemical characteristics as the descriptors. Tian et al. [22] utilized the decision tree, kernel ridge regressor, Gaussian process regressor, and K nearest neighbors to build machine learning models with good performance, in which the top-important descriptors were filtered out in advance by using the decision tree and univariate selection. However, the machine learning models usually suffer from the lack of sufficient experimental data or the inconsistency between data from different references. Moreover, the descriptors including the physical, chemical, and material properties of ITR, such as

4

the melting point, heat capacity, unit cell volume, density, and film thickness play dominant role in the IRT prediction, the selection of which may limit the accuracy of the models for application in composite materials.

The method based on parametric fitting with respect to experimental observables has been used to estimate the ITR in composite materials. In the method, the effect of ITR on thermal conductivity is represented by the models such as effective medium theory (EMT) model [23] , Hashin-Shtrikman model [24] and Hamilton-Hasselman model [25]. The value of ITR is determined by fitting the parameters of the model with respect to the experimental measurements such as effective thermal conductivity, filler size, volume fraction, etc. The method was usually used in experimental works to give rough estimation of how the ITR changes with respect to different experimental treatment to composite samples. For accurate estimation, the method suffers from the limitation of the theoretical models. For example, EMT considers the composite with single type of filler, Hashin-Shtrikman model only gives the relative ITR that is not comparable to other models; extra uncertainties can be introduced when the structure of composite becomes complex [26, 27], such as when fillers are not evenly distributed and with various shapes. Replacing the theoretical models with numerical modeling certainly improves the flexibility of the representation of various composite materials. Nevertheless, noises and fluctuations of properties introduced by the numerical modeling make the parametric fitting tricky.

In this paper, we propose an innovative strategy for an accurate determination of ITR in particle-laden composites taking the advantage of high-throughput calculation, machine learning and experiments (see in Fig. 1). Firstly, a series of standard samples with randomly dispersed fillers are fabricated in experiments, whose thermal conductivities are characterized with sufficient statistics. The corresponding numerical models of the standard samples are generated in terms of the statistics of the fillers in experiments. The structures of the models are compared with the nano-CT of the standard samples to guarantee the fidelity. Then high-throughput calculations with the numerical modeling based on fast Fourier transform algorithm algorithm areare carried out to build a database containing the input variables of modeling and the corresponding output effective thermal conductivities. The input variables include the respective thermal conductivity of the fillers and polymer matrix, and the respective ITR for interfaces of filler-polymer (ITR_{f-p}) and filler-filler (ITR_{f-f}). The obtained database is used to train a prototypical function-based machine learning model to represent the quan-

titative relationship between the input and output variables, $\kappa = f(\text{ITR}_{f-p}, \text{ITR}_{f-f})$, where κ denotes the effective TC of the composites. Then the ITRs in the particle-laden composites is determined by a high-throughput screening of the independent variables of $\kappa = f(\text{ITR}_{f-p}, \text{ITR}_{f-f})$, taking the effective TCs of the standard samples measured in experiments as references. Finally, the determined ITRs are validated by comparing between the numerical predictions and the experiments of the validation samples. The proposed methodology provides a versatile tool for accurate determination of ITRs inside composite materials, which could also enable a further high-throughput screening of design parameters of composite materials based on numerical modeling with high accuracy.
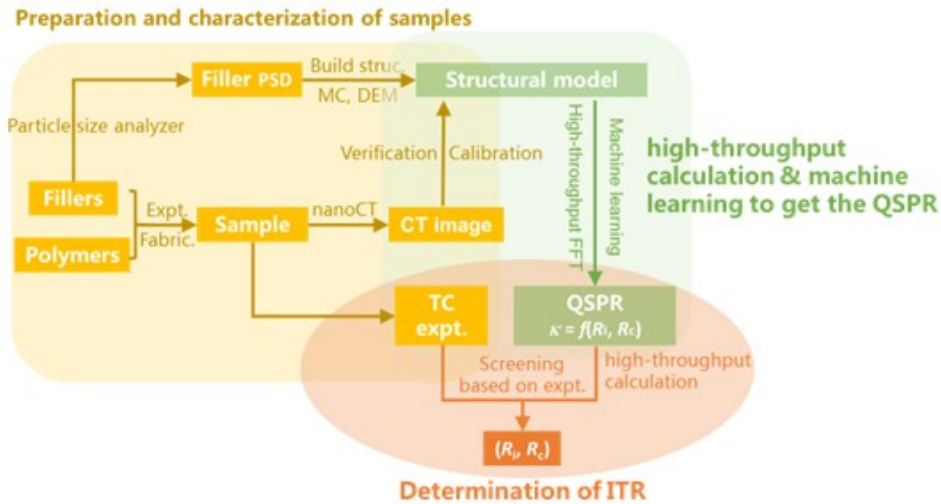
Figure 1: Strategy of the proposed algorithm for the determination of ITR.

2. Results

2.1. Measurement of size distribution of fillers

We first measure the statistics of the fillers, which will be used to build microscopic structures of the composites for numerical modeling. The particulate fillers are AlN and Al_2O_3 with average particle size of 3 and 4 μm, respectively. The particle size distribution is measured with Malvern Panalyticle particle size analyzer (Type: Mastersizer 3000), with the results shown in Fig. 2. It shows that the experimental data of particle diameter D obeys

6

logarithmic normal distribution in Eq. (1), which is the common distribution in the industrial powder products:

$$f(D) = \frac{1}{D * \sigma * \sqrt{2\pi}} \exp(-(\log D - \mu)^2 / 2\sigma^2). \tag{1}$$

The parameters μ and σ for Al_2O_3 and AlN are determined by fitting the data with logarithmic normal distribution, from which we can deduce the arithmetic mean E[D] and arithmetic standard deviation SD[D] as:

$$E[D] = \exp(\mu + \frac{\sigma^2}{2}). \tag{2}$$

$$SD[D] = E[x] * \sqrt{\exp(\sigma^2) - 1}. \tag{3}$$

The values are given in Table. 1.
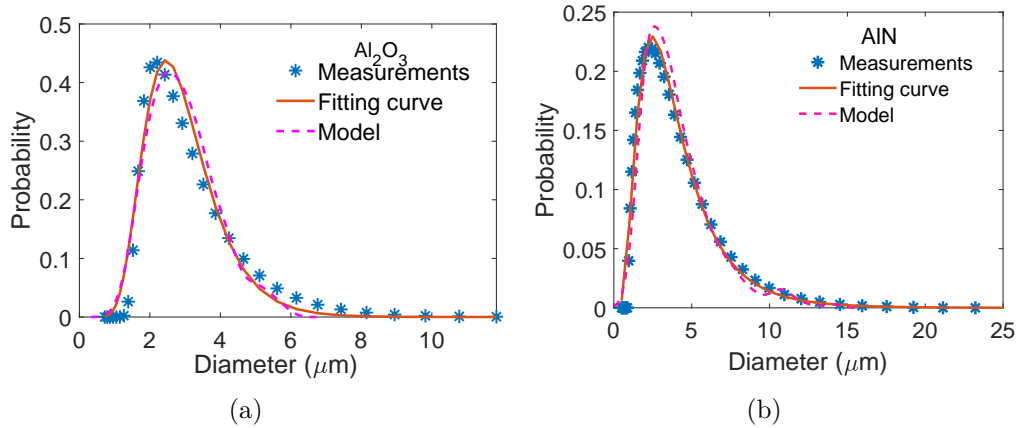
Figure 2: Particle size distribution of (a) Al_2O_3; (b) AlN.

Table 1: The fitting parameters and characteristic parameters for the particle size.

Type	μ (μm)	σ (μm^2)	E[D] (μm)	SD[D] (μm^2)
Al_2O_3	1.02	0.35	2.95	1.06
AlN	1.25	0.59	4.17	2.70

2.2. Preparation of composite samples and characterization of structures

Silicone is selected as the polymer matrix of the standard samples of the thermally conductive composite materials. The silane coupling agent is employed to promote the dispersion of the particulate fillers in the composites.

The Al_2O_3-x/silicone, AlN-y/silicone and Al_2O_3-x-AlN-y/silicone composites are prepared by a mixing process, where x and y denote the absolute volume fraction of Al_2O_3 and AlN in the composites, respectively. The fillers, coupling agent and silicone matrix are weighted properly and mixed under vacuum in the high-speed mixer with a speed of 1500 r/min for 2 minutes. The various filler volume fractions of the composite samples are listed in Table. 2. Note that the coupling agent occupies 4 vol% in all these samples. The 3D images of the composites are obtained with the X-ray micro-CT (YXLON FF20 CT), from which both the distribution of filler sizes and positions can be derived. The information will be used to validate the microscopic structures of the numerical models for the composites.

Table 2: The details of samples with various filler volume fractions.

Samples	Al_2O_3 volume fraction (x vol%)	AlN volume fraction (y vol%)
Al_2O_3-x/silicone	55, 58, 60, 65	0
AlN-y/silicone	0	55, 58, 60, 62
Al_2O_3-x-AlN-y/silicone	29	29
	30	30
	31	31
	32.5	32.5

2.3. Measurement of TC of composite samples

The thermal conductivities of the standard samples are measured by LW-9389 TIM Thermal Conductivity and Resistance Tester, which will act as references for the determination of ITRs. For each formula in Table. 2, we prepare four independent samples and measure the respective thermal conductivity (Table. 3), from which the mean and variance of the measurements are derived. It can been seen that the variance of the Al_2O_3/silicone samples is smaller than that of the AlN/silicone ones, which is attributed to the better dispersion of Al_2O_3 particles. The dispersion of the particulate fillers can be validated by micro-CT test. For instance, Fig. 3 presents the micro-CT images of an Al_2O_3-60/silicone sample in which the red points denote the Al_2O_3 particles, showing a random and uniform distribution.

8

Table 3: The thermal conductivities of the standard samples measured by experiment technique.

| Samples	Thermal conductivity (W/mK)					
	1	2	3	4	Average	Variance
Al_2O_3-55/silicone	1.29	1.30	1.22	1.32	1.28	0.0019
Al_2O_3-58/silicone	1.57	1.46	1.47	1.42	1.48	0.0041
Al_2O_3-60/silicone	1.56	1.56	1.50	1.48	1.53	0.0017
Al_2O_3-65/silicone	1.96	1.98	2.01	1.93	1.97	0.0011
AlN-55/silicone	1.54	1.62	1.40	1.51	1.52	0.0083
AlN-58/silicone	1.77	1.61	1.83	1.56	1.69	0.0164
AlN-60/silicone	1.90	1.85	1.93	1.89	1.89	0.0011
AlN-62/silicone	2.32	2.30	2.46	2.38	2.37	0.0052
Al_2O_3-29-AlN-29/silicone	1.49	1.48	1.45	1.47	1.47	0.0003
Al_2O_3-30-AlN-30/silicone	1.64	1.74	1.68	1.48	1.64	0.0124
Al_2O_3-31-AlN-31/silicone	1.65	1.69	1.82	1.84	1.75	0.0089
Al_2O_3-32.5-AlN-32.5/silicone	2.00	2.18	2.32	2.09	2.15	0.0186
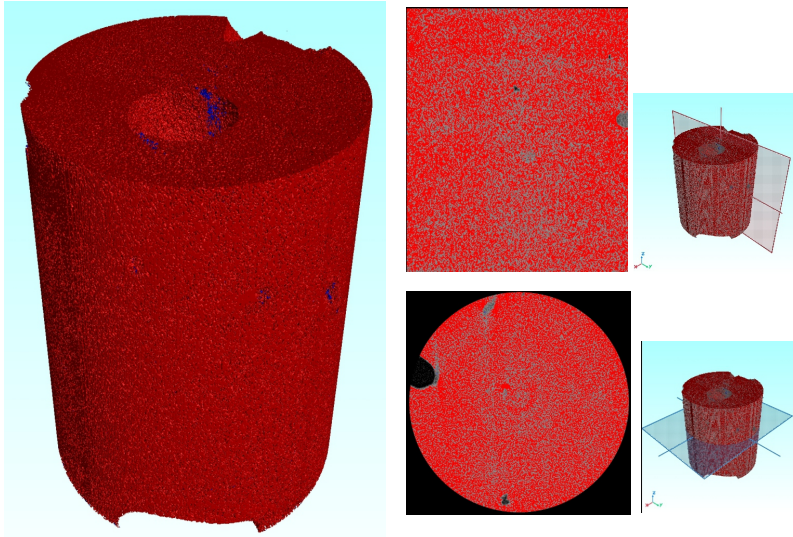
Figure 3: The micro-CT image of Al_2O_3-60/silicone sample.

2.4. Generation of microstructures for numerical modeling

The microstructures of the particulate composites are generated by using GrainGeo module of GeoDict software (Math2Market GmbH, Germany)

9

based on the measured statistics of the fillers used in the standard samples. The representative volume element (RVE) is a cubic box meshed with unit cells (voxels), and the side length of the RVE is 40 μm. The side length of the cubic voxels of RVE is 0.1 μm, with the number of voxels being $400 \times 400 \times 400$. The Al_2O_3 and AlN particles of the measured size distribution as shown in Fig. 2 and Table. 1 are dispersed randomly without overlapping in the RVE under periodic boundary condition. Various microstructures of the composites are generated according to the gradation in Table. 2, including the Al_2O_3/silicone, AlN/silicone and Al_2O_3-AlN/silicone composites. Several examples of the microstructures with different filler volume fractions are presented in Fig. 4, where the red and blue particles denote Al_2O_3 and AlN, respectively. The sizes of the particles in the models are extracted and the corresponding particle size distribution is compared with the experimental data, showing a good agreement (see in Fig. 2). It indicates that the generated structures of the composites are consistent with the reality. The selection of gradation schemes for the microstructures is addressed in the next section.
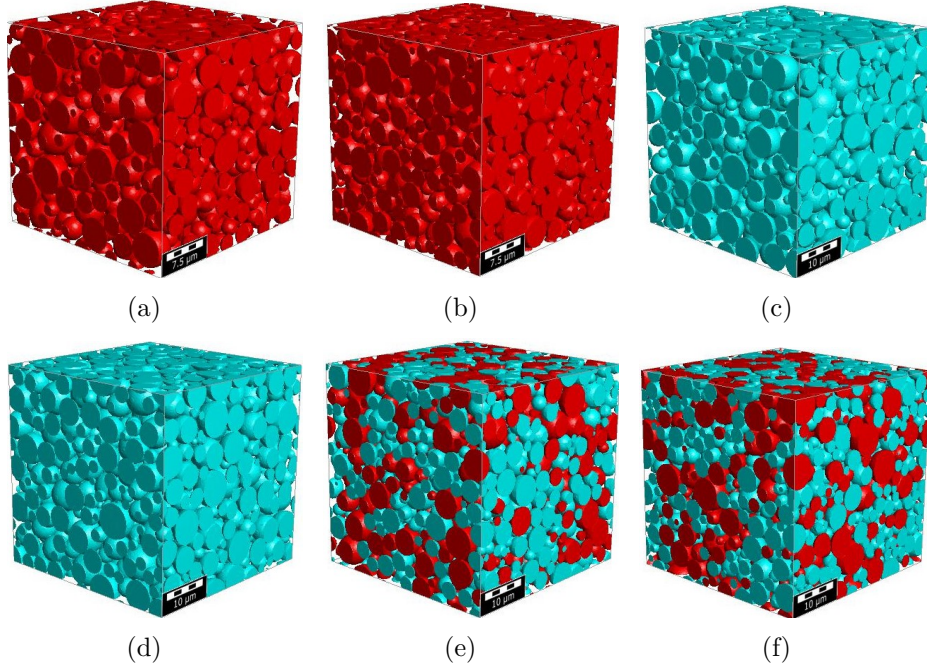
Figure 4: Microstructures of the particulate composites, where the red and blue particles denote Al_2O_3 and AlN, respectively. (a) Al_2O_3-55; (b) Al_2O_3-65; (c) AlN-55; (d)AlN-60; (e) Al_2O_3-30-AlN-30; (f) Al_2O_3-32.5-AlN-32.5.

2.5. Determination of quantitative relationship between ITR and TC of composites

The quantitative relationship between the ITR and effective TC of the composite, κ=f(ITR_{f-p}, ITR_{f-f}), are represented by a machine learning model trained based on a database obtained from high-throughput calculations, where κ, ITR_{f-p}, and ITR_{f-f} denote the effective TC of composite, the ITRs for filler-polymer and filler-filler interfaces, respectively. The High-throughput calculations are realized by using the ConductoDict module of GeoDict software and a home-made Python post-processing script. GeoDict calculates the TC tensors based on the so-called explicit jump immersed interface approach, which solves the equations in parallel by combing the fast Fourier transform (FFT) and GiGGStab methods. We have recently shown that the approach dramatically reduces the computational time and requirement of memory without losing precision compared with the finite element modeling, which enables the efficient and accurate high-throughput calculations [28]. The input parameters for the numerical simulations are the TCs

11

of the fillers, the ITR between the fillers and silicone matrix (ITR_{f-p}), and the ITR between the fillers (ITR_{f-f}). A range of different values are selected for each input variable (Table. 4), based on which the high-throughput calculations are performed. The range of values for each variable is set to be reasonable based on the physics. As a result, a total of 320 simulations are conducted for the composite with single type of filler (i.e., Al_2O_3-x/silicone or AlN-y/silicone), each of which has 3 input variables (TC of filler, ITR_{f-p}, and ITR_{f-f}). For the composites with both Al_2O_3 and AlN as fillers (i.e.,Al_2O_3-x-AlN-y/silicone), however, there will be seven input variables resulting in 819200 combinations according to Table 4, which is prohibitively expensive to simulate. Therefore, only five types of ITRs with reduced range of values (see S4 in SI) are selected as the input variables for the simulation, which reduces the number of simulations to 2048. The TCs of Al_2O_3 and AlN are set as 30 and 200 W/mK in the simulations of the binary mixed particle-filled composites, respectively, which are based on the intrinsic properties of the commercial samples. Besides, the TC of silicone matrix is set as a constant of 0.18 W/mK, which is not selected as an input variable.

Table 4: Input parameters for the high-throughput computations.

Parameter	Selected values
$k_{silicone}$ (W/mK)	0.18
$k_{Al_2O_3}$ (W/mK)	20, 25, 30, 35, 40
k_{AlN} (W/mK)	150, 180, 200, 220, 250
$R_{Al_2O_3-Silicone}$ (m^{2}K/W)	10^{-8}, 5×10^{-8}, 10^{-7}, 5×10^{-7}, 10^{-6},5×10^{-6}, 10^{-5}, 5×10^{-5}
$R_{AlN-Silicone}$ (m^{2}K/W)	10^{-8}, 5×10^{-8}, 10^{-7}, 5×10^{-7}, 10^{-6},5×10^{-6}, 10^{-5}, 5×10^{-5}
$R_{Al_2O_3-Al_2O_3}$ (m^{2}K/W)	10^{-8}, 5×10^{-8}, 10^{-7}, 5×10^{-7}, 10^{-6},5×10^{-6}, 10^{-5}, 5×10^{-5}
$R_{AlN-AlN}$ (m^{2}K/W)	10^{-8}, 5×10^{-8}, 10^{-7}, 5×10^{-7}, 10^{-6},5×10^{-6}, 10^{-5}, 5×10^{-5}
$R_{Al_2O_3-AlN}$ (m^{2}K/W)	10^{-8}, 5×10^{-8}, 10^{-7}, 5×10^{-7}, 10^{-6},5×10^{-6}, 10^{-5}, 5×10^{-5}

The results of the high-throughput simulations serve as the database for the machine learning. Fig. 5 illustrates the prototypical function-based machine learning framework for constructing the predicting model for the quantitative relation κ=f(ITR_{f-p}, ITR_{f-f}), where κ, ITR_{f-p}, and ITR_{f-f} denote the effective TC of composite, the ITRs of the filler-polymer and filler-filler interfaces, respectively. In order to best represent the quantitative relationship with limited set of training data, we train the machine learning model separately for the systems with different volume fraction of fillers, instead of

constructing a general predicting model. The volume fractions selected for the training can be found in Table. 2. Taking the binary mixed particle-filled composite as an example, the 5 kinds of ITRs in Table. 4 are chosen as 5 features $(x_1, x_2, ..., x_5)$ for the machine learning model; for each feature, 12 prototypical functions (Fig. 5) are generated following the work of Shen et al.[29]. Among the 12 prototypical functions of each feature, we choose the top 3 best prototypical functions by comparing the coefficient of determination (R^2) generated by the least squares regression (LSR). Those 3 prototypical functions for each feature are taken as the representatives for that feature to describe the quantitative relationship κ=f(ITR$_{f-p}$, ITR$_{f-f}$). Then we conduct combinations among the 5 features, each of which represented by the respective top 3 selected prototypical functions, to get 31 combinations in total ($x_1 x_2, x_1 x_3, ..., x_1 x_2 x_3, ..., x_1 x_2 x_3 x_4 x_5$, see S5 in SI in detail). Note that the single feature, such as x_1, is also treated as a special case of the combination. For each type of combination, we choose the top 3 best combined prototypical functions according to the LSR, same as the previous step, which gives a total of 15 combined prototypical functions. Finally, the quantitative κ=f(ITR$_{f-p}$, ITR$_{f-f}$) are determined by using curve_fit method with the 15 prototypical functions as inputs [30]. For the composite material with single type of filler, such as Al_2O_3/silicone and AlN/silicone, the number of features reduces to 3, which include the intrinsic TC of the filler and the ITRs of the filler-polymer and filler-filler interfaces. All other procedures for determining the machine learning model are the same as those for the binary mixed particle-filled system; the only difference is that the TCs of the fillers are considered as features here, whereas they are constants at the intrinsic TC of that material for the machine learning of the composite with both Al_2O_3 and AlN, aiming to reduce the number of features. The details of the expression of the machine learning models for κ=f(ITR$_{f-p}$, ITR$_{f-f}$) are provided in Supplementary information. The machine learning models are validated by comparing the predictions with the numerical simulations for a variety of different systems, as shown in Fig. 6. The R^2 of all the predictions are between 0.9671 and 0.9954, demonstrating the high quality of the machine learning models.

2.6. Determination of interfacial thermal resistance (ITR)

The ITRs between components inside the composites are determined by the high-throughput screening of the input parameters of the machine learning models, κ=f(ITR$_{f-p}$, ITR$_{f-f}$), taking the experimental effective TCs of
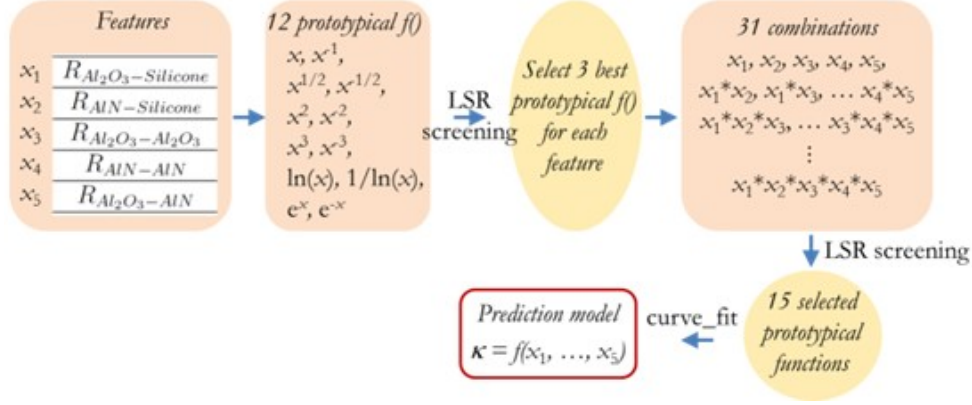
Figure 5: Workflow of the machine learning algorithm employed in the present work.

the standard samples as the references (see in Fig. 7). In practice, the ITRs are determined in a hierarchical manner; the ITR_{f-p} ($R_{Al_2O_3-Silicone}$ and $R_{AlN-Silicone}$) and ITRs between the same types of fillers ($R_{Al_2O_3-Al_2O_3}$ and $R_{AlN-AlN}$) are first determined based on the composites with a single type of filler; then the determined ITRs are used as known parameters in the binary mixed particle-filled composites, from which we determine the ITRs between the different types of fillers ($R_{Al_2O_3-AlN}$). Taking Al_2O_3/silicone composites as example, we change the interfacial thermal resistances $R_{Al_2O_3-Silicone}$ and $R_{Al_2O_3-Al_2O_3}$ from 10^{-8} to 10^{-5} m^{2}K/W at a step of one tenth of the magnitude of values while fixing the thermal conductivity of Al_2O_3 particles at 30 W/mK leading to 7344 combinations of the input parameters. Note that the TCs of fillers are treated as known parameters, though they are independent variables in the machine learning models for the composites with a single type of filler. The effective TCs of the composites with several filler volume fractions (55%, 60% and 65% for the Al_2O_3/silicone composite) are computed with the machine learning model based on the different ITRs as input parameters. We define the error of the machine learning prediction as

$$\delta = \sqrt{\sum_{f=vol\%} (\boldsymbol{k}_f^{ML} - \boldsymbol{k}_f^{exp})^2}. \tag{4}$$

where k_f^{ML} and k_f^{expt} are the effective TCs of the composite with filler volume fraction of f from the machine learning prediction and experimental measurement of the standard sample (Table. 3), respectively. By finding the minimum values of δ, the corresponding input parameters are determined
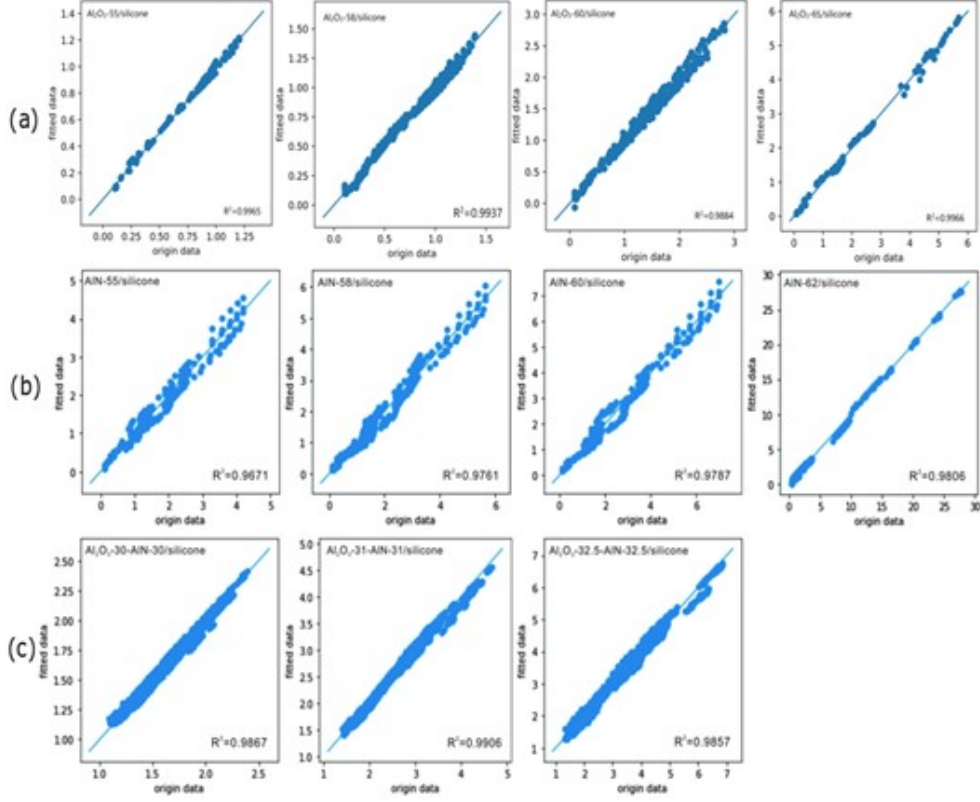
14

Figure 6: Comparisons of thermal conductivity between the numerical simulation and the machine learning prediction for (a) Al_2O_3/silicone composites (b) AlN/silicone composites (c) Al_2O_3-x-AlN-y/silicone composites with various filler volume fraction, where x and y denote the volume percentage of Al_2O_3 and AlN particles respectively.

as the ITRs of $R_{Al_2O_3-Silicone}$ and $R_{Al_2O_3-Al_2O_3}$. Following the same procedure we determine $R_{AlN-Silicone}$ and $R_{AlN-AlN}$ based on the AlN/silicone systems with AlN volume fractions of 58%, 60% and 62%. The TC of AlN particles is chosen as 200 W/mK in computing the effective TCs of the AlN-filled composites. The obtained ITRs are then used as known parameters for computing the effective TCs of the Al2O3-x-AlN-y/silicone composite systems with the (x, y) selected as (31%, 31%) and (32.5%, 32.5%), based on which the $R_{Al_2O_3-AlN}$ is screened out from the range between 10^{-8} and 10^{-5} m^2K/W.

The cumulative frequency of the error δ for determining the ITRs are shown in Fig. 8. It should be noted that the figure for each material system
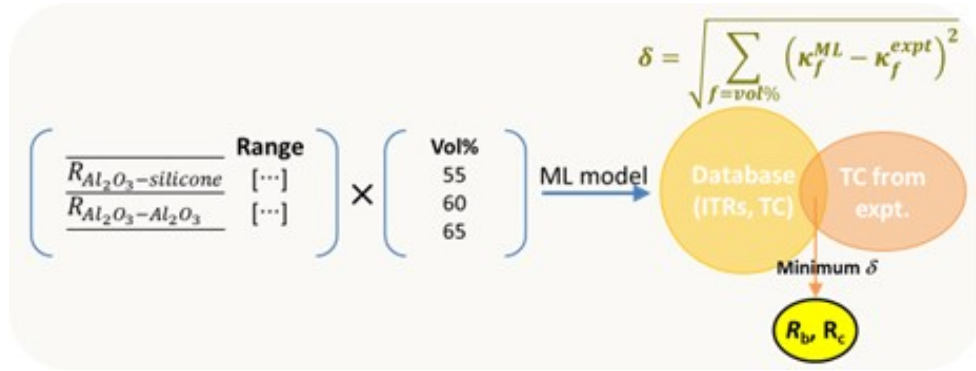
Figure 7: Scheme for the determination of ITR.

corresponds to the summation of δ under various volume fractions with the same input parameters. For the determination of ITRs for each system, we select the values of δ below 1% of the cumulative frequency, the corresponding input parameters of which are the range of ITRs. The determined values of the ITRs are shown in Table. 5.
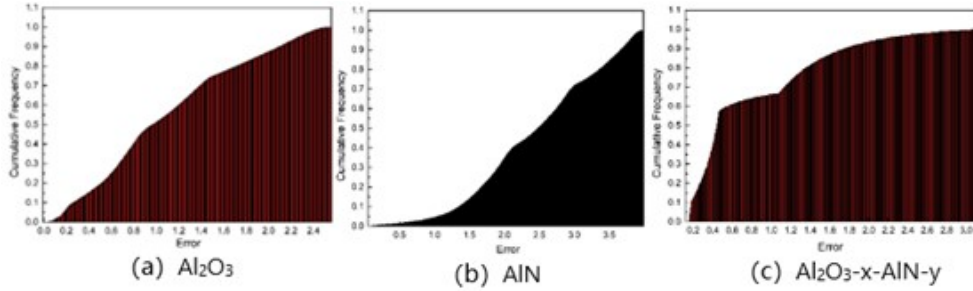

Figure 8: Cumulative frequency of the error δ used for determining the ITR

Table 5: The summary of the determined interfacial thermal resistance.

Type of interfacial thermal resistance	Values (m^2K/W)$\pm$10%
Al_2O_3-silicone	2.2×10^{-8}
AlN-silicone	3.0×10^{-8}
Al_2O_3-Al_2O_3	2.0×10^{-7}
AlN-AlN	1.0×10^{-7}
Al_2O_3-AlN	3.0×10^{-7}

16

2.7. Validation of accuracy of the determined interfacial thermal resistance

Finally the determined ITRs are validated by comparing between the numerical predictions and the experiments of the validation samples. The proposed methodology provides a versatile tool for accurate determination of ITRs inside composite materials, which could also enable a further high-throughput screening of design parameters of composite materials based on numerical modeling with high accuracynd.

To validate the accuracy of identified interfacial thermal resistance, a comparison between the numerical predictions and the experiment measurements is presented in Table. 6. For each test sample in Table. 6, 3 independent random microstructures are generated and the thermal conductivities along three main directions are computed taken into account the interfacial thermal resistance in Table. 5, whose average is compared with the averaged measured results of 4 random samples. The relative error between the numerical prediction and experimental measurement is given as

$$E_R = \frac{|\bar{k}_f^{num} - \bar{k}_f^{expt}|}{\bar{k}_f^{expt}} \times 100\% \tag{5}$$

The results in Table. 6 indicate that the relative errors are all below 10 %, i.e., the accuracy of the numerical prediction is higher than 90 %.

Table 6: Comparison between the measured and predicted thermal conductivities of the standard samples.

Samples	Thermal conductivity (W/mK)		Relative error
	Measured results $\bar{k}_f^{expt}$	Numerical prediction $\bar{k}_f^{num}$	
Al$_2$O$_3$-55/silicone	1.28	1.17	8.59%
Al$_2$O$_3$-58/silicone	1.48	1.40	5.41%
Al$_2$O$_3$-60/silicone	1.53	1.56	1.96%
Al$_2$O$_3$-65/silicone	1.97	2.14	8.63%
AlN-55/silicone	1.52	1.37	9.87%
AlN-58/silicone	1.69	1.68	0.59%
AlN-60/silicone	1.89	2.00	5.82%
AlN-62/silicone	2.37	2.38	0.42%
Al$_2$O$_3$-29-AlN-29/silicone	1.47	1.42	3.40%
Al$_2$O$_3$-30-AlN-30/silicone	1.64	1.61	1.83%
Al$_2$O$_3$-31-AlN-31/silicone	1.75	1.84	5.14%
Al$_2$O$_3$-32.5-AlN-32.5/silicone	2.15	2.25	4.65%

3. Discussion

3.1. Relationship between R_b and R_c

From Table. 5, it can be noted that the contact resistance between the particles is always higher than the interfacial thermal resistance between particle and matrix. Here we provide a reasonable explanation for this phenomenon. In the particulate composites system, the interfacial thermal resistance between the particles and matrix, R_b, is assumed as an extremely thin layer which is characterized by an imperfect interface as shown in Fig. 9 (a). Specifically, through the interfacial thermal resistance interface between the particle and matrix, the temperature is continuous while the heat flux along the normal direction of the interface suffers a jump. However, the contact resistance between the particles in the present work, R_c, consists of the contributions of two particle-matrix interface resistance as well as a thin matrix layer between the particles as depicted in Fig. 9 (b).

$$R_c = 2R_b + R_{silicone} \tag{6}$$

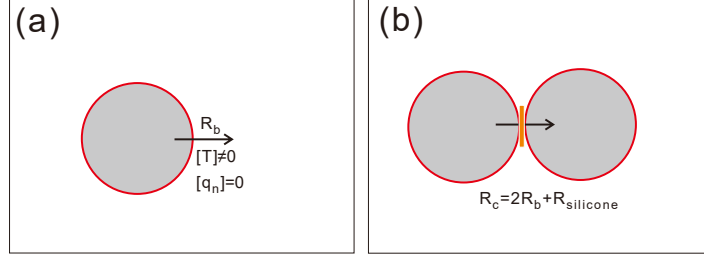Therefore, it is obvious that R_c should always be higher than R_b.

18

Figure 9: Scheme of the interfacial thermal resistance between particle and matrix R_b, and the interfacial thermal resistance between particles R_c.

3.2. Comparison with previously reported values

There are quite few work about the identification of interfacial thermal resistance related with Al_2O_3 or AlN, with which we can make a comparison. Li et al.[31] measured the ITR between Ni and Al_2O_3 by 3ω method, showing a result of 6.8×10^{-9} m^2K/W. Fabrizio Iacobazzi et al.[32] employed diffuse mismatch model to calculate the ITR between Al_2O_3 and oil, water and ice respectively. The corresponding values of the ITRs are between $7\sim8\times10^{-10}$ m^2K/W. The ITR between Al_2O_3 and polymer is much higher, as the measurement of Putman et al.[33] for the interface thermal resistance between Al_2O_3 and PMMA, which is $(3.75\pm1.25)\times10^{-8}$ m^2K/W. It coincides with our identification of ITR between Al_2O_3 and Silicone shown in Table 9. Moreover, the ITR in the AlN/PI composites has been determined by fitting the curve of theoretical model with the experimental data of thermal conductivity of the composites [34], giving a result of 3.32×10^{-7} m^2K/W. It should be noted that this value corresponds to the interfacial thermal barrier resistance parameter in the modified Maxwell's equation, which consists of the influence of both the filler-matrix ITR and filler-filler ITR. Thus, it is higher than our estimation of ITR between AlN and silicone, which is 1×10^{-7} m^2K/W.

3.3. Comparison with other machine learning algorithms

Aside from the prototypical function-based machine learning strategy, we also tried several other machine learning algorithms to train the database of high-throughput computations, such as the eXtreme Gradient Boosting (XGBoost) model, Support Vector Regression (SVR), and Artificial Neural Network (ANN) methods. The XGBoost model is a type of gradient boosting

model designed by Tianqi Chen [35], which is an integrated learning algorithm based on decision tree with high accuracy and improved computational efficiency. In the field of composite materials, many researchers have used XGBoost to carry out relevant research. For instance, Furtado et al. [36] presented a feasibility study on the application of XGBoost to predict the design-allowed notch strength of multidirectional composite laminates. Milad et al.[37] used XGBoost to design a prediction model for the strain of fiber-reinforced polymer (FRP) composites based on 729 experimental data whose influential parameters include material geometry, strength properties, strain properties, FRP properties and confinement properties. SVR is also a widely used machine learning algorithm which maps data to high-dimensional feature space through nonlinear mapping, and realizes linear regression transformation from nonlinear function estimation problem to high-dimensional feature space. Wei et al.[38] predicted the effective thermal conductivity of composites and porous media by SVR, showing a better performance than the traditional analytical models in terms of predicting accuracy. Sultana et al.[39] employed three different algorithms, i.e., Response Surface Methodology (RSM), ANN and SVR, to develop nonlinear empirical models for the prediction of mechanical properties of Jute Fiber Reinforced Concrete Composites. The results demonstrate that SVR model performs better than ANN and RSM models. ANN abstracts the human brain neuron network from the perspective of information processing, offering a complicated correlation between variables of input and output. The ANN models were successfully used for predicting various phenomena in polymer composites. Liang et al.[40] accurately predicted the thermal conductivity of BN polymer composites by using a semi-supervised artificial neural network model with a collaborative training style, in which the thermal conductivity of polymer matrix, the diameter, aspect ratio, and volume fraction of the BN sheets are considered as the input variables of the thermal conduction model.. Luo et al.[41] employed ANN to build the correlation models between the cured shape types and ply-stacking sequences of the carbon/epoxy composite laminates, which can give a rapid and accurate prediction of the cured shapes than conventional finite element method.

Fig. 10 shows the accuracy of XGBoost model for Al_2O_3-55/silicone and Al_2O_3-65/silicone composites respectively. The values of R^2 are higher than 0.99, showing a good agreement between the testing data and the predictions by XGBoost. However, when we continue the high-throughput screening of the interfacial thermal resistance based on XGBoost model, it turns out the

problem of precision. Specifically, when we fix the thermal conductivity of Al_2O_3 as well as the Al_2O_3-silicone interfacial thermal resistance, and vary the Al_2O_3-Al_2O_3 interfacial thermal resistance from 2.0×10^{-8} to 2.9×10^{-8} m^2K/W, the values of effective thermal conductivity predicted by the trained XGBoost model are the same. Thus, this algorithm is not suitable for our dataset.

In Fig. 11, we predict the thermal conductivity of Al_2O_3/silicone composites using SVR and ANN, and compare the results with original data by numerical simulation. It can be seen that the R^2 scores obtained from the two methods are 0.8312 and 0.716 respectively, and the predicted results are far from the accurate data. This demonstrates that the SVR method and ANN method do not have the capability in predicting the effective thermal conductivity of composite materials with good accuracy when the input parameter are sensitive interfacial thermal resistance. Overall, due to the limitations of XGBoost, SVR and ANN as mentioned above, we confirm that the prototypical function-based machine learning strategy is the best choice in solving our problem.
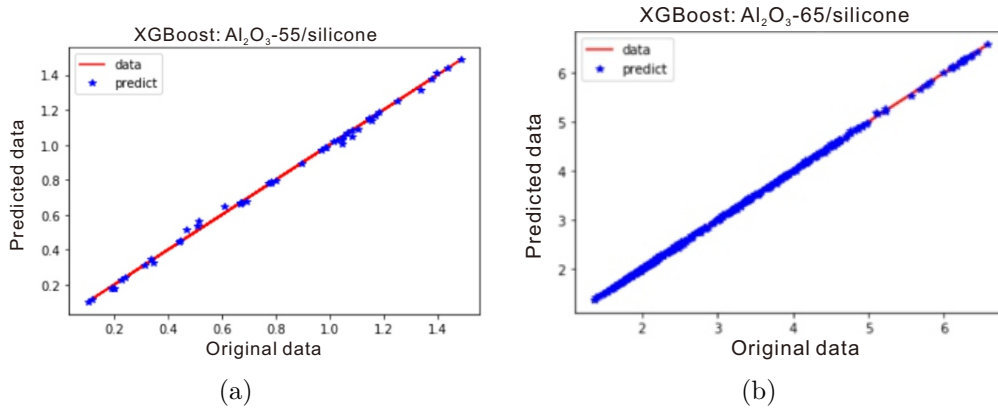

Figure 10: Comparisons of thermal conductivity between the training data by numerical simulation and the predictions by XGBoost model for (a) Al_2O_3-55/silicone composites and (b) Al_2O_3-65/silicone composites.
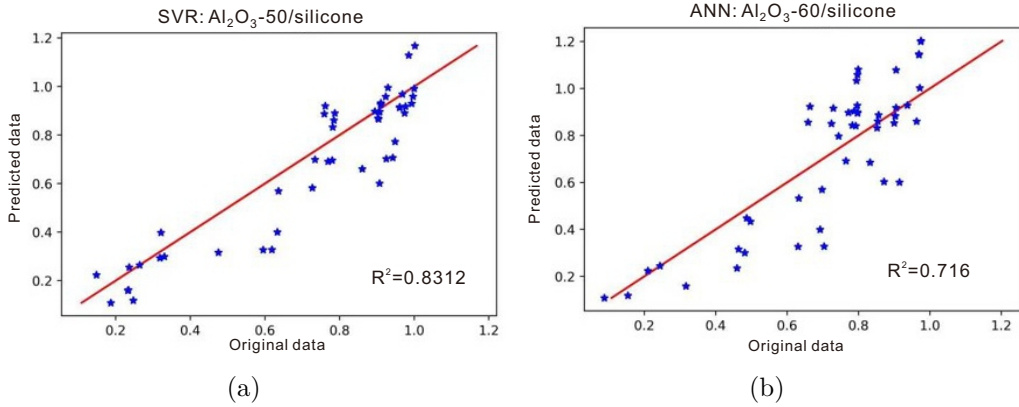
Figure 11: Comparisons of thermal conductivity between the training data by numerical simulation and the predictions by (a) SVR model for Al_2O_3-50/silicone composites and (b) ANN method for Al_2O_3-60/silicone composites.

4. Conclusion

In this paper, we proposed an efficient method to identify the interfacial thermal resistance in particle-laden composites combining the numerical simulation, high-throughput computation, machine learning algorithm and simple experimental measurement. Firstly, the corresponding numerical model is generated according to the designed standard samples, following by high-throughput computations of the effective thermal conductivity. The independent input parameters of the numerical simulation are the thermal conductivity of particulate fillers as well as the particle-matrix and particle-particle interfacial thermal resistances. Then, the obtained database is trained by a prototypical function-based machine learning strategy which gives us the numerical relation between the input parameters and the effective thermal conductivities. Finally, a high-throughput screening of the input parameters is conducted comparing the experimental measurement results of effective thermal conductivities with the predictions from machine learning model for the standard samples, by which we are able to identify the interfacial thermal resistance in the particulate composites. The the computational cost of the innovative strategy is negligible compared to the direct measurements of interfacial thermal resistance such as microthermal bridge method.

To fully illustrate the application of the strategy, we present an example of the identification of interfacial thermal resistances in Al_2O_3-AlN/silicone composites, following by a convincing validation. Meanwhile, other machine

learning algorithms, such as XGBoost, SVR and ANN, are also tested, showing limitations in solving our problem. We conclude that the prototypical function-based machine learning strategy we employed is the best choice to train the database in this work. Our work demonstrates that the high-throughput computations combined with machine learning methods can be used as a fast prediction tool to obtain the interfacial thermal resistance in particle-laden composites, which can overcome the difficulties of complex operations in micro-scaled measurement and the high error of analytical calculation based on physics.

5. Methods

Thermal conductivity of the particulate composites is measured by a LW-9389 TIM Thermal Conductivity and Resistance Tester (Long Win Science and Technology Corporation, Taiwan). The thermal conductivity is calculated from the following Eq. (7):

$$K = \frac{Qt}{A\Delta T} \tag{7}$$

where Q is the heat flux, ΔT is the temperature difference between temperature sensors of meter bar, t is the thickness of the specimen and A is the sample surface area. In order to eliminate the influence of thermal resistance between the specimen and the meter bar on the thermal conductivity of the specimen, we conducted three tests for each specimen at various thickness: t=0.5 mm, 1.0 mm and 1.5 mm, respectively. The resulting thermal impedance I of the tests versus the thickness of the specimen satisfies linear relationship, which can be fitted as

$$I = at + b \tag{8}$$

Here a and b are fitting parameters. The thermal impedance is given as

$$I = \frac{A\Delta T}{Q}. \tag{9}$$

Thus, we can deduce the absolute thermal conductivity of the specimen without the effect the interfacial thermal resistance induced from the testing process,

$$K = 1/a. \tag{10}$$

6. Aknowledgements

DATA AVAILABILITY STATEMENT

Research data are not shared.

References

[1] A. L. Moore, L. Shi, Emerging challenges and materials for thermal management of electronics, Materials Today 17 (4) (2014) 163–174.

[2] K. M. Razeeb, E. Dalton, G. L. W. Cross, A. J. Robinson, Present and future thermal interface materials for electronic devices, International Materials Reviews 63 (1) (2018) 1–21.

[3] C. P. Feng, L. Bai, R.-Y. Bao, S.-W. Wang, Z. Liu, M.-B. Yang, J. Chen, W. Yang, Superior thermal interface materials for thermal management, Composites Communications 12 (2019) 80–85.

[4] Y. Guo, K. Ruan, X. Shi, X. Yang, J. Gu, Factors affecting thermal conductivities of the polymers and polymer composites: A review, Composites Science and Technology 193 (2020) 108134.

[5] E. T. Swartz, R. O. Pohl, Thermal boundary resistance, Rev. Mod. Phys. 61 (1989) 605–668.

[6] X. Xu, J. Chen, J. Zhou, B. Li, Thermal conductivity of polymers and their nanocomposites, Advanced Materials 30 (17) (2018) 1705544.

[7] R. Prasher, Predicting the thermal resistance of nanosized constrictions, Nano Letters 5 (11) (2005) 2155–2159.

[8] P. Reddy, K. Castelino, A. Majumdar, Diffuse mismatch model of thermal boundary conductance using exact phonon dispersion, Applied Physics Letters 87 (21) (2005) 211908.

[9] L. Ren, Q. Chen, Study on the interfacial thermal resistance between cnts and al with a ttm-md model, Molecular Physics 119 (6) (2021) e1851417.

[10] F. Meng, M. Elsahati, J. Liu, R. F. Richards, Thermal resistance between amorphous silica nanoparticles, Journal of Applied Physics 121 (19) (2017) 194302.

[11] X. Ran, Y. Wang, J. Lu, R. Sun, J.-B. Xu, N. Yang, H. Yin, C.-P. Wong, Effect of hydrogen bonds on the thermal transport in a precisely branched polyethylene with ordered and amorphous structures, Computational Materials Science 205 (2022) 111191.

[12] W. Dai, L. Le, J. Lu, H. Hou, CTL, A paper-like inorganic thermal interface material composed of hierarchically structured graphene/silicon carbide nanorods, ACS Nano 13 (2) (2019) 1547–1554.

[13] N. Yang, X. Zeng, J. Lu, R. Sun, C. P. Wong, Effect of chemical functionalization on the thermal conductivity of 2d hexagonal boron nitride, Applied Physics Letters 113 (17) (2018) 171904.

[14] A. Kumar, N. Ayyagari, T. S. Fisher, Effects of graphene nanopetal outgrowths on internal thermal interface resistance in composites, ACS Applied Materials & Interfaces 8 (10) (2016) 6678–6684.

[15] K. Pietrak, T. S. Wiśniewski, M. Kubiś, Application of flash method in the measurements of interfacial thermal resistance in layered and particulate composite materials, Thermochimica Acta 654 (2017) 54–64.

[16] K. Zheng, J. Zhu, Y.-M. Ma, D.-W. Tang, F.-S. Wang, Interfacial thermal resistance between high-density polyethylene (HDPE) and sapphire, Chinese Physics B 23 (10) (2014) 107307.

[17] E. Chapelle, B. Garnier, B. Bourouga, Interfacial thermal resistance measurement between metallic wire and polymer in polymer matrix

composites, International Journal of Thermal Sciences 48 (12) (2009) 2221–2227.

[18] J. González, A. Bedoya, A. Mendioroz, A. Salazar, Measuring the thermal resistance of vertical interfaces separating two different media using infrared thermography, International Journal of Thermal Sciences 135 (2019) 410–416.

[19] Q.-Y. Li, K. Katakami, T. Ikuta, M. Kohno, X. Zhang, K. Takahashi, Measurement of thermal contact resistance between individual carbon fibers using a laser-flash raman mapping method, Carbon 141 (2019) 92–98.

[20] M. L. Fitzgerald, Y. Zhao, Z. Pan, L. Yang, S. Lin, G. Sauti, D. Li, Contact thermal resistance between silver nanowires with poly(vinylpyrrolidone) interlayers, Nano Letters 21 (10) (2021) 4388–4393.

[21] Y.-J. Wu, L. Fang, Y. Xu, Predicting interfacial thermal resistance by machine learning, npj Computational Materials 5 (1) (2019) 1–8.

[22] X. Tian, M. Chen, Descriptor selection for predicting interfacial thermal resistance by machine learning methods, Scientific reports 11 (1) (2021) 1–10.

[23] F. Deng, Q.-S. Zheng, L.-F. Wang, C.-W. Nan, Effects of anisotropy, aspect ratio, and nonstraightness of carbon nanotubes on thermal conductivity of carbon nanotube composites, Applied Physics Letters 90 (2) (2007) 021914.

[24] I.-L. Ngo, S. Prabhakar Vattikuti, C. Byon, A modified hashin-shtrikman model for predicting the thermal conductivity of polymer composites reinforced with randomly distributed hybrid fillers, International Journal of Heat and Mass Transfer 114 (2017) 727–734.

[25] W. Jiajun, Y. Xiao-Su, Effects of interfacial thermal barrier resistance and particle shape and size on the thermal conductivity of aln/pi composites, Composites Science and Technology 64 (10) (2004) 1623–1628.

[26] Tong, Zhen, Liu, Meng, Bao, Hua., A numerical investigation on the heat conduction in high filler loading particulate composites., International Journal of Heat & Mass Transfer 100 (2016) 355–361.

[27] S. Zhai, P. Zhang, Y. Xian, J. Zeng, B. Shi, Effective thermal conductivity of polymer composites: Theoretical models and simulation models, International Journal of Heat and Mass Transfer 117 (2018) 358–374.

[28] X. Lu, X. Fu, J. Lu, R. Sun, J. Xu, C. Yan, C. P. Wong, Numerical homogenization of thermal conductivity of particle-filled thermal interface material by fast fourier transform method, Nanotechnology 32 (26) (2021) 265708 (12pp).

[29] Z.-H. Shen, J.-J. Wang, J.-Y. Jiang, S. X. Huang, Y.-H. Lin, C.-W. Nan, L.-Q. Chen, Y. Shen, Phase-field modeling and machine learning of electric-thermal-mechanical breakdown of polymer-based dielectrics, Nature communications 10 (1) (2019) 1–10.

[30] Scipy documentation.(n.d.), `https://docs.scipy.org/doc/scipy/reference/generated/scipy.optimize.curve_fit.html` (2021).

[31] X. Li, W. Park, Y. P. Chen, X. Ruan, Absence of coupled thermal interfaces in al2o3/ni/al2o3 sandwich structure, Applied Physics Letters 111 (14) (2017) 143102.

[32] F. Iacobazzi, M. Milanese, G. Colangelo, M. Lomascolo, A. de Risi, An explanation of the al2o3 nanofluid thermal conductivity based on the phonon theory of liquid, Energy 116 (2016) 786–794.

[33] S. A. Putnam, D. G. Cahill, B. J. Ash, L. S. Schadler, High-precision thermal conductivity measurements as a probe of polymer/nanoparticle interfaces, Journal of Applied Physics 94 (10) (2003) 6785–6788.

[34] W. Jiajun, Y. Xiao-Su, Effects of interfacial thermal barrier resistance and particle shape and size on the thermal conductivity of aln/pi composites, Composites Science and Technology 64 (10-11) (2004) 1623–1628.

[35] T. Chen, C. Guestrin, Xgboost: A scalable tree boosting system, in: Proceedings of the 22nd ACM SIGKDD International Conference on

Knowledge Discovery and Data Mining, Association for Computing Machinery, New York, NY, USA, 2016, p. 785–794.

[36] C. Furtado, L. Pereira, R. Tavares, M. Salgado, F. Otero, G. Catalanotti, A. Arteiro, M. Bessa, P. Camanho, A methodology to generate design allowables of composite laminates using machine learning, International Journal of Solids and Structures 233 (2021) 111095.

[37] A. R. K. M. R. H. A.-M. A. Milad, S. H. Hussein, T. H. Tran, Development of ensemble machine learning approaches for designing fiber-reinforced polymer composite strain prediction model, Engineering with Computers (2021) 1–13.

[38] H. Wei, S. Zhao, Q. Rong, H. Bao, Predicting the effective thermal conductivities of composite materials and porous media by machine learning methods, International Journal of Heat and Mass Transfer 127 (2018) 908–916.

[39] N. Sultana, S. Zakir Hossain, M. S. Alam, M. Islam, M. A. A. Abtah, Soft computing approaches for comparative prediction of the mechanical properties of jute fiber reinforced concrete, Advances in Engineering Software 149 (2020) 102887.

[40] Y. Liang, Z. Liu, W. Liu, A co-training style semi-supervised artificial neural network modeling and its application in thermal conductivity prediction of polymeric composites filled with bn sheets, Energy and AI 4 (2021) 100052.

[41] L. Luo, B. Zhang, G. Zhang, Y. Xu, Rapid prediction of cured shape types of composite laminates using a fem-ann method, Composite Structures 238 (2020) 111980.